Original

Li, D.; Storch, H.v.; Geyer, B.:

High-resolution wind hindcast over the Bohai Sea and the Yellow Sea in East Asia: Evaluation and wind climatology analysis

Journal of Geophysical Research : Atmospheres (2016) AGU

DOI: 10.1002/2015JD024177

AGU PUBLICATIONS

JGR

Journal of Geophysical Research: Atmospheres

RESEARCH ARTICLE
10.1002/2015JD024177

Key Points:
- CCLM is robust to reproduce the regional wind characteristics over the BYS
- Added value is generated along coastal areas with complex orography
- Wind speed has significant positive trends in south YS in winter and spring

Correspondence to:
D. Li,
delei.li@hzg.de

Citation:
Li, D., H. von Storch, and B. Geyer (2016), High-resolution wind hindcast over the Bohai Sea and the Yellow Sea in East Asia: Evaluation and wind climatology analysis, *J. Geophys. Res. Atmos.*, *121*, 111–129, doi:10.1002/2015JD024177.

Received 6 SEP 2015
Accepted 5 DEC 2015
Accepted article online 12 DEC 2015
Published online 7 JAN 2016

High-resolution wind hindcast over the Bohai Sea and the Yellow Sea in East Asia: Evaluation and wind climatology analysis

Delei Li[1], Hans von Storch[1,2], and Beate Geyer[1]

[1]Helmholtz-Zentrum Geesthacht Centre for Materials and Coastal Research, Geesthacht, Germany, [2]Center of Excellence CliSAP, University of Hamburg, Hamburg, Germany

Abstract A 34 year (1979–2012) high-resolution (7 km grid) atmospheric hindcast over the Bohai Sea and the Yellow Sea (BYS) has been performed using COSMO-CLM (CCLM) forced by ERA-Interim reanalysis data (ERA-I). The accuracy of CCLM in surface wind reproduction and the added value of dynamical downscaling to ERA-I have been investigated through comparisons with the QuikSCAT Level2B 12.5 km version 3 (L2B12v3) swath data and in situ observations. The results revealed that CCLM has a reliable ability to reproduce the regional wind characteristics over the BYS. Added value to ERA-I has been detected in the coastal areas with complex orography. CCLM wind quality had strong seasonal variability, with better performance in the summer relative to ERA-I, even in the offshore areas. CCLM was better able to represent light and moderate winds but had even more added value for strong winds relative to ERA-I. The spatial digital filter method was used to investigate the scale of the added value, and the results show that CCLM adds value to ERA-I mainly in medium scales of wind variability. Furthermore, wind climatology was investigated, and significant increasing trends in the south Yellow Sea especially in winter and spring were found for seasonal mean wind speeds.

1. Introduction

Wind is a fundamental element in climate systems. Wind describes climate variability and change in itself and is a determinant factor of other environmental elements [*Wan et al.,* 2010]. Generally, wind is generated because of horizontal differences in air pressure, and therefore, it reflects the atmosphere circulation. Wind also greatly influences the transfer of heat, energy, water, and momentum both in horizontal and vertical directions, which factors greatly in land-atmosphere, ocean-atmosphere, and land-ocean interaction systems. Specifically, marine surface winds induce ocean general circulation as well as ocean wave and upwelling and downwelling processes and also contributes to the tide surges. The prediction of waves or storm surges depends on the quality of surface wind conditions. From an academic point of view, it is fundamental to have a robust wind data set and an investigation of wind variability and change, which is also of great importance to economic and social activities. A number of human activities and applications in coastal and offshore areas are greatly affected by marine wind conditions, especially extreme wind events, including coastal defence infrastructure, wind farm construction, oil platform installations, shipment routing, and tourism and leisure activities.

Therefore, a long-term and homogeneous surface wind data set is necessary to derive wind statistics, including wind variability, climate change, and extreme events. However, those types of data are generally unavailable over marine areas.

Surface wind data can be obtained from station observations. Observation-based studies aim to accurately investigate wind variability at local or regional levels, with the assumption that the local observation is representative of wind conditions in some area around the site and, likewise, that the integration of local information leads to regional wind characteristics [*Jiménez et al.,* 2010]. Unfortunately, observational data are sensitive to changes in observation instruments, the exposure of the observation site, recording procedures, and other factors [*Aguilar et al.,* 2003], and thus, temporal inhomogeneity prevails for many local wind observations. Furthermore, the construction of observation stations, especially over marine areas, such as meteorological masts or buoy stations, is too expensive and needs frequent maintenance. Some alternatives are necessary to obtain wind data sets.

Satellite observations represent one alternative option for wind studies. With advanced satellite techniques, ocean surface wind studies are highly enhanced because spatial wind maps from satellites provide more

information on ocean surface winds than isolated station observations [*Alvarez et al.,* 2013]. Scatterometer satellites, such as the Quik Scatterometer (QuikSCAT) and advanced scatterometer, provide global wind data with resolutions of 12–50 km and have been used to investigate the spatial and temporal variability of ocean surface winds from regional to global levels [e.g., *Risien and Chelton,* 2008; *Kara et al.,* 2009; *Bentamy et al.,* 2012]. However, the satellite wind data suffer from short-time records as well as irregular observations at spatial and temporal scales. Therefore, over the past decades, there has been increasing interest in using a numerical method to obtain long-term and homogeneous wind data sets.

Reanalysis is a method to objectively combine observations and numerical models for an integrated estimate of the system state. The products are thought to be the best estimates of many variables, such as temperature and winds [*Portoghese et al.,* 2013]. However, the reanalysis data sets generally have coarse resolution, leading to a poor ability to resolve regional wind features, especially for areas with complex orography.

To achieve much finer spatial and temporal features at regional or local levels, downscaling from general circulation models (GCMs) or global atmospheric reanalyses has been performed. Downscaling approaches include statistical, dynamical, and combined statistical-dynamical downscaling. For dynamical downscaling, a limited area model or regional climate model (RCM) is employed to obtain climate variability with finer spatial and temporal resolution of an area of interest [*Hong and Kanamitsu*, 2014; *Xue et al.,* 2014]. A crucial issue related to dynamical downscaling is whether RCM can add value to its forcing data set. In past years, great efforts have been devoted to investigating the skill and performance of dynamical RCMs and the added value to their driving data set. The results demonstrate that they can realistically simulate weather or climate variability and change at a range of locations across the world, including but not limited to Europe, Africa, East Asia, and North America; however, debate remains focused on the added value issue [*Feldmann et al.,* 2008; *Feser and von Storch*, 2008; *Panitz et al.,* 2013; *Wang et al.,* 2013; *Lee et al.,* 2013, 2014; *Geyer*, 2014; *Lee and Hong*, 2014; *Wang and Kotamarthi*, 2014]. Furthermore, most of the studies have traditionally focused on precipitation and air temperature. When it comes to the studies of surface winds, in recent decades, several studies have been performed on simulation reliability as well as the added value of RCMs to their forcing data sets [*Sotillo et al.,* 2005; *Winterfeldt and Weisse*, 2009; *Reistad et al.,* 2011; *Winterfeldt et al.,* 2011; *Pryor et al.,* 2012; *Menendez et al.,* 2013; *Li et al.,* 2015].

Sotillo et al. [2005] validated the spectrally nudged regional climate simulation with the regional climate model REMO against the NCEP1 reanalysis [*Kalnay et al.,* 1996], and the results show that the spectrally nudged REMO introduced a substantial enhancement over the NCEP1 reanalysis in 10 m wind fields, especially over the complex orography of the Mediterranean area. *Winterfeldt et al.* [2011] demonstrated that the regional model had an added value to the reanalysis wind forcing in the coastal areas of European waters with complex orography by comparing it with QuikSCAT Level 2B 12.5 km data sets. *Pryor et al.* [2012] assessed the influence of horizontal resolution on simulated wind climates over northern Europe. Their results indicated that there is no uniform improvement for power spectra of the simulated surface winds with an increase in model resolution, and the model resolution appears to have a greater impact on wind climate extremes than on mean wind speeds. *Menendez et al.* [2013] developed two hindcast products with different temporal and spatial resolutions over the entire Mediterranean Sea; when validated against in situ station and satellite data, a good agreement between wind hindcasts and measurements was shown. *Li et al.* [2015] validated the robustness of different reanalyses in constraining dynamical downscaling by assessing coastal winds in East Asia and revealed that the newer generation reanalyses, such as the ERA-I [*Dee et al.,* 2011] and the Japanese 55 year Reanalysis [*Kobayashi et al.,* 2015], outperform the older generation reanalysis NCEP1 [*Kalnay et al.,* 1996] in high-resolution downscaling applications.

In this paper, we consider the Bohai Sea (BS) and the Yellow Sea (YS) areas in East Asia (Figure 1). We use the abbreviation BYS to refer to both BS and YS. The BS is a semienclosed sea within China, with the Liaodong Peninsula (LDP) bordering to the east and the Shandong Peninsula (SDP) to the south. The YS is a much larger marginal sea, which is connected to the BS to the north and to the East China Sea to the south, with the Korean Peninsula (KP) bordering to the east and mainland China to the west. The coastal areas of the BYS are characterized by remarkably dense populations. They are significant areas for agriculture, fisheries, industry, and tourism. However, human populations and properties in these areas are greatly threatened by many natural hazards, such as cyclones, storm surges, and extreme waves. It is imperative to comprehensively investigate the coastal and offshore climate of the BYS; however, such a study has been unavailable until now. This study aims to contribute to climate studies over the BYS, focusing on marine surface winds.

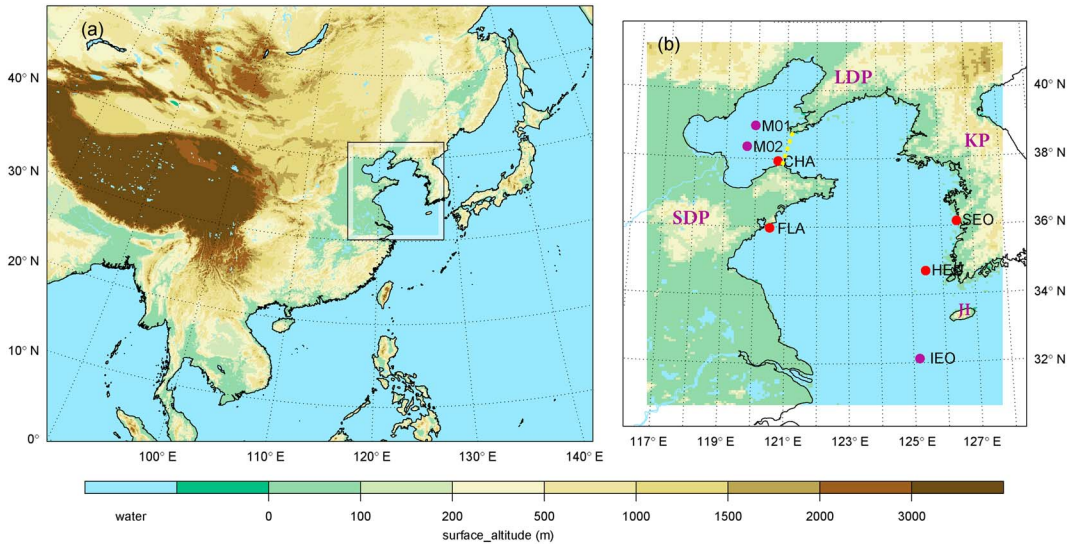

Figure 1. (a) Geographical location of the Bohai Sea and the Yellow Sea (rectangle) in East Asia, (b) Orography of the simulation domain: red points indicate coastal stations, and dark magenta refers to offshore stations. The border between the Bohai Sea and the Yellow Sea is marked with a yellow dashed line. SDP, LDP, KP, and JI represent the Shandong Peninsula, Liaodong Peninsula, Korean Peninsula, and Jeju Island, respectively.

In the present study, a high-resolution (approximately 7 km grid) long-term wind simulation driven by ERA-Interim [*Dee et al.,* 2011] (hereafter called ERA-I) is assessed by comparing it against in situ and satellite wind observations. We determined the added value constructed by implementing the dynamical downscaling step for the description of wind conditions compared to ERA-I. Before providing details on the added value assessment, a definition should be given. As illustrated by *Di Luca et al.* [2015], several definitions of added value are used in the RCM community, including but not limited to observational added value, conjectural added value, and potential added value. In the present study, the term observational added value is used, which is straightforward, simple, and widely used in assessing RCMs by calculating some metric scores and comparing them to the forcing data set.

The paper is organized as follows. Section 2 describes the forcing reanalysis data set, the hindcast simulation, the observational data sets, and the evaluation methods used in the study. The evaluation and added value issues of CCLM are considered in section 3. Section 4 includes the analysis of the wind conditions, in terms of means, variability, and trends. The discussion and conclusions are in section 5.

2. Data Sets and Method

2.1. Global Reanalysis Data

The global atmospheric reanalysis ERA-I [*Dee et al.,* 2011, 2014], a third-generation reanalysis, is produced by the European Centre for Medium Range Weather Forecasts (ECMWF). It covers the period from 1 January 1979 to the present, with extensions forward in near-real time. The horizontal spatial resolution of ERA-I is approximately 80 km (T255 spectral), the temporal output interval is 6 h, and it has 60 levels vertically from the surface up to 0.1 hPa. A four-dimensional variational analysis (4D-Var) was adopted to produce ERA-I, with much improvement over earlier reanalysis, such as ERA-40 [*Uppala et al.,* 2005], in terms of low-frequency variability, the hydrological cycle, temporal consistency, and the quality of stratospheric circulation.

2.2. Regional Atmospheric Hindcast

The nonhydrostatic regional climate model CCLM (COSMO-CLM) [*Rockel et al.,* 2008] [http://www.clm-community.eu/] version 4.14 is used to perform the regional climate hindcast over BYS. The CCLM is the climate version of the COSMO weather prediction model, which was developed by Deutscher Wetterdienst.

The temporal integration of the simulation is carried out using the Runge-Kutta scheme with a time step of 60 s. The initial and boundary conditions, as well as the spectrally nudging constraints of the hindcast simulation, are provided by the reanalysis ERA-I with 6-hourly update frequencies. The interior spectral nudging

Table 1. List of Wind Speed Observation Sites and Their Locations (Longitude, Latitude), Observation Periods, Numbers of Valid Pairs (Number), and Observation Heights

Station	Longitude (°E)	Latitude (°N)	Period	Number	Height (m)
		Coastal Measurement			
CHA	120.717	37.933	1986/01–2010/12	59816	40
FLA	120.483	35.967	1979/01–2002/06	15241	25
HEU	125.451	34.687	2001/07–2010/12	26888	68.5
SEO	126.50	36.13	2005/01–2007/08	15822	3
		Offshore Measurement			
M01	119.950	38.967	1988/10–2000/04	4351	6
M02	119.683	38.350	1986/05–1993/12	8014	6
IEO	125.18	32.12	2005/01–2007/03	11099	42

technique [*von Storch et al.,* 2000] is applied at every third time step on the horizontal wind fields with levels above 850 hPa. It can keep the model solution close to the forcing at large scales and develop local or regional scale processes on its own, whereas for the standard boundary forcing technique, the internal state of the regional model conflicts with the large-scale state of the forcing data. Land surface conditions, such as land-sea masks, soil types, and vegetation, are provided by the CLM community (http://www.clm-community.eu/). The horizontal resolution is 0.0625° (approximately 7 km), with 168×190 grid points in the longitudinal and latitudinal directions, and 10 grid boxes are set as a sponge zone at the lateral boundary at each side (Figure 1). The choice of horizontal resolution is based on setup experiences with COSMO weather prediction models as well as the balance between overall experiment design and computational performance. There are 40 levels in the vertical direction. Various physical parameterizations are used. The TERRA-ML scheme [*Schrodin and Heise*, 2002] is used for land surface processes. The cumulus convection is parameterized based on *Tiedtke* [1989] and the radiation scheme from *Ritter and Geleyn* [1992]. A Kessler-type scheme [*Kessler*, 1969] is used for microphysics, including snow and cloud ice processes.

2.3. Observation Data

Two types of observational data are used to verify the simulated winds: QuikSCAT satellite data and in situ wind data from buoys, tower, and platform stations (Table 1).

2.3.1. QuikSCAT Satellite Data

The QuikSCAT satellite is in a Sun-synchronous orbit. Each orbit lasts 100 min, and the travelling speed is 7 km s^{-1}. The data set product used here is the latest reprocessed version 3 of the QuikSCAT Level 2B wind data (QuikSCAT L2BV3), which is provided on a nonuniform grid within the swath at a 12.5 km pixel resolution. It has several improvements over the previous QuikSCAT L2B winds, including changes in measurement binning, the application of improved Geophysical Model Function, the correction of rain contaminated winds, and the discarding of cross track depended wind speed biases. The product demonstrates reliable quality, with root-mean-square errors of wind speeds (direction) at 1.5 m s^{-1} (17°) when compared to both numerical weather products (ECMWF, rain-free day) and buoy observations [*Fore et al.,* 2014].

To verify the simulated wind speeds, some preprocessing work has been conducted to colocate the QuikSCAT L2BV3 swath data to the CCLM grid (Figure 1). QuikSCAT measurements within a half-grid mesh size (approximately 3.5 km) in the longitude and latitude directions from the CCLM grid points and 10 min from the simulated full hour are averaged and assigned as "observations" for the simulated grid. All QuikSCAT measurements below 3 or above 25 m s^{-1} are not used in the colocation procedure because of the limited quality of light and extreme winds [e.g., *Hoffman and Leidner*, 2005; *Winterfeldt et al.,* 2011; *Moroni et al.,* 2013]. Eventually, a grid data set was generated extending across 10 years from December 1999 to November 2009, which is hereafter named QuikSCAT.

2.3.2. In Situ Data

Observation wind data recorded at seven stations are obtained from the National Marine Data and Information Service of China (NMDIS) and the National Climatic Data Center (NCDC) of the United States. The in situ data are divided into two types, coastal and offshore measurements, based on the distances of their locations to the coastline (Figure 1b). Detailed information is given in Table 1. For comparisons with the simulated wind speeds, the observational wind data are converted to a height of 10 m, taking into consideration the wave dependence of the roughness length via the Charnock relation [*Stull*, 1988].

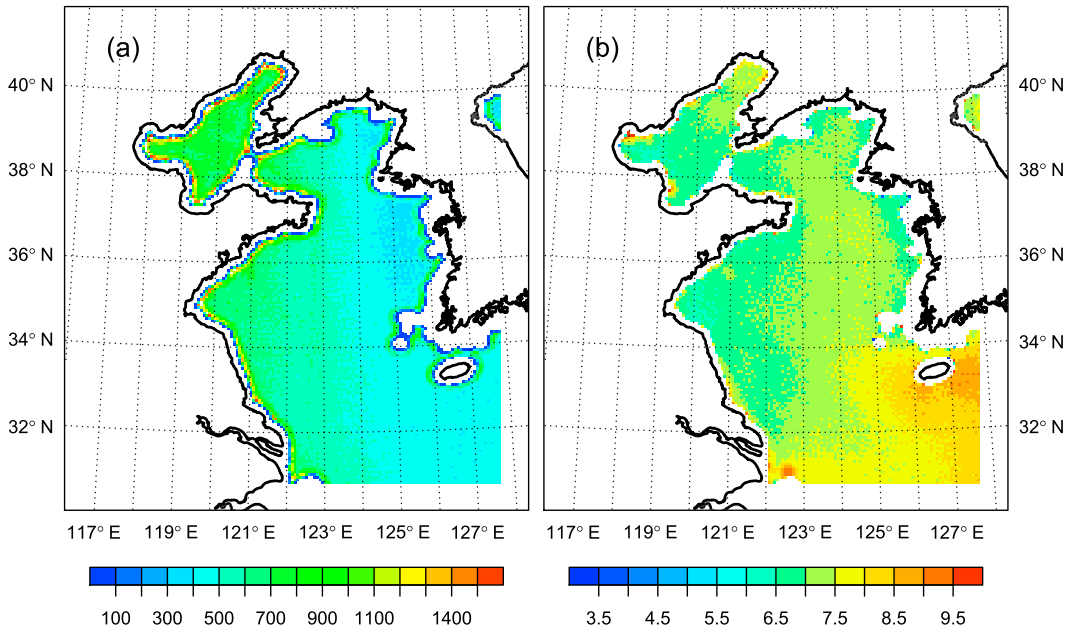

Figure 2. (a) Number of valid colocations between CCLM and QuikSCAT data for wind speeds range of 3–25 m s^{-1}, (b) Mean wind speeds of colocated QuikSCAT (3–25 m s^{-1}) data during December 1999 and November 2009.

2.4. Evaluation Methods

For comparisons with CCLM wind data, the coarse-resolution (6-hourly frequency and approximately 80 km spatial resolution) ERA-I wind data are interpolated to hourly data in time and to the CCLM grid. When compared with station observation data, ERA-I and CCLM grid data are interpolated to the stations' locations using the nearest-neighbor method. Only simultaneous pairs between modelled winds (ERA-I, CCLM) and observed winds are selected for the verification process. When compared against the satellite data, ERA-I and CCLM data are spatially and temporally masked based on the availability of QuikSCAT data (3–25 m/s).

Several statistical measures are used to evaluate the quality of modelled wind speeds, including mean bias (Bias), correlation coefficient (Corr), root mean square error (RMSE), standard deviation (SD), and the normalized RMSE by SD (NRMSE). Furthermore, modified Brier Skill Score (BSS) [e.g., *Winterfeldt et al.,* 2011] is used to assess the added value from dynamical downscaling in comparison with the driving reanalysis ERA-I:

$$\mathrm{BSS} = \begin{cases} 1 - \sigma^2(x_C, x_Q)/\sigma^2(x_E, x_Q) & \text{if} \quad \sigma^2(x_C, x_Q) \le \sigma^2(x_E, x_Q) \\ \sigma^2(x_E, x_Q)/\sigma^2(x_C, x_Q) - 1 & \text{if} \quad \sigma^2(x_C, x_Q) > \sigma^2(x_E, x_Q) \end{cases}, \tag{1}$$

where $\sigma(x_C, x_Q)$ and $\sigma(x_E, x_Q)$ represent the error standard deviations of the CCLM wind speeds (x_C) and the ERA-I wind speeds (x_E), respectively, and x_Q refers to the QuikSCAT wind speeds. The BSS value ranges from −1 to 1: a negative value indicates that ERA-I fits better to QuikSCAT than CCLM, and positive values mean that there is added value in the CCLM winds compared to ERA-I wind speeds.

Sen's slope estimator [*Sen*, 1968] is used to assess the linear trend magnitudes of wind speeds over the BYS. The estimator is the median one among slopes determined by all pairs of sample points. The Mann-Kendall significance test (MK test) [*Mann*, 1945; *Kendall*, 1948] has been used to test the significance of trend. The test generally assumes that the data are independently and identically distributed, which is generally not the case for climate data. The existence of serial correlation in the climate data will increase the probability of significant trends detected by the MK test [e.g., *von Storch*, 1995]. In other words, in application, significant trends detected by the MK test may be generated either because of the real trend signal or merely because the data are serially correlated [*Blain*, 2013]. To limit the influence of serial correlation on the MK test, the Yue-Pilon prewhitening method [*Yue et al.,* 2002] has been used in our study to remove lag-one autoregressive processes and obtain independent series for the MK test.

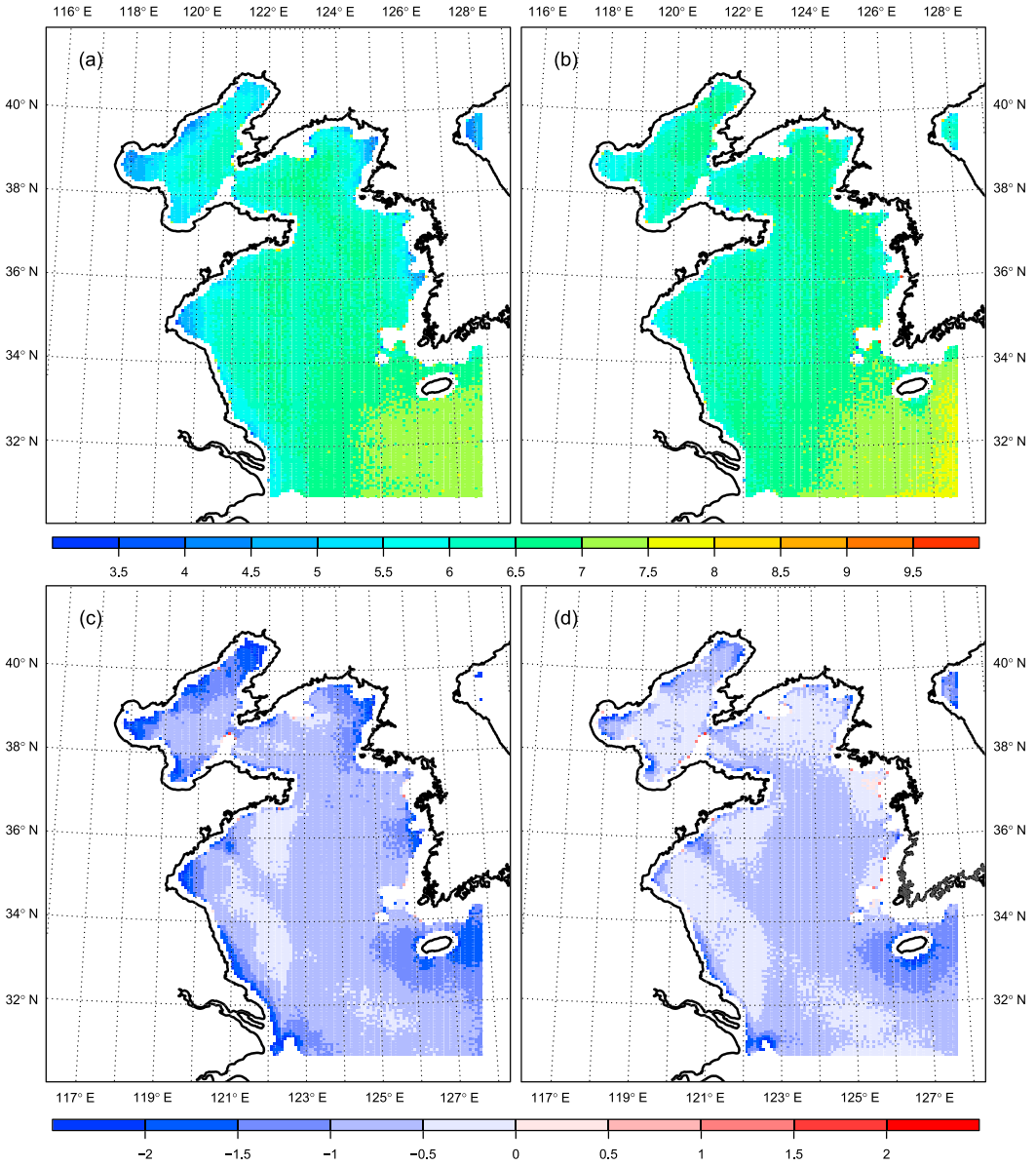

Figure 3. Colocated mean wind speeds ($m\,s^{-1}$) for (a) ERA-I, (b) CCLM, and the bias of colocated mean wind speeds between (c) ERA-I and QuikSCAT and between (d) CCLM and QuikSCAT.

3. Results

3.1. General Assessment of CCLM Wind Hindcast

The number of valid co-locations between CCLM and QuikSCAT for wind speeds between 3 and 25 $m\,s^{-1}$ during the 10 year period (December 1999 to November 2009) varies from 400 to 750 (Figure 2). More colocations are in the western coastal area (more than 550) than in the eastern area (less than 500), which is due to the orbit specification of QuikSCAT, which results in better coverage by scatterometer swaths for the western area than the eastern area. Furthermore, coastline or island contaminations of backscatter measurements lead to the unavailability of QuikSCAT in near coastal regions, especially for the coastal area of the Korean Peninsula (Figure 2a), where the coastline is complex and islands are widely distributed. Although we mainly investigate the QuikSCAT winds in the range of 3 to 25 $m\,s^{-1}$ in this study, we have determined the proportions of colocated wind speeds less than 3 $m\,s^{-1}$ as 10% to 20% of all colocations for most parts of the BYS and 5% to 10% for the southeastern part but more than 20% for the northeastern corner of YS.

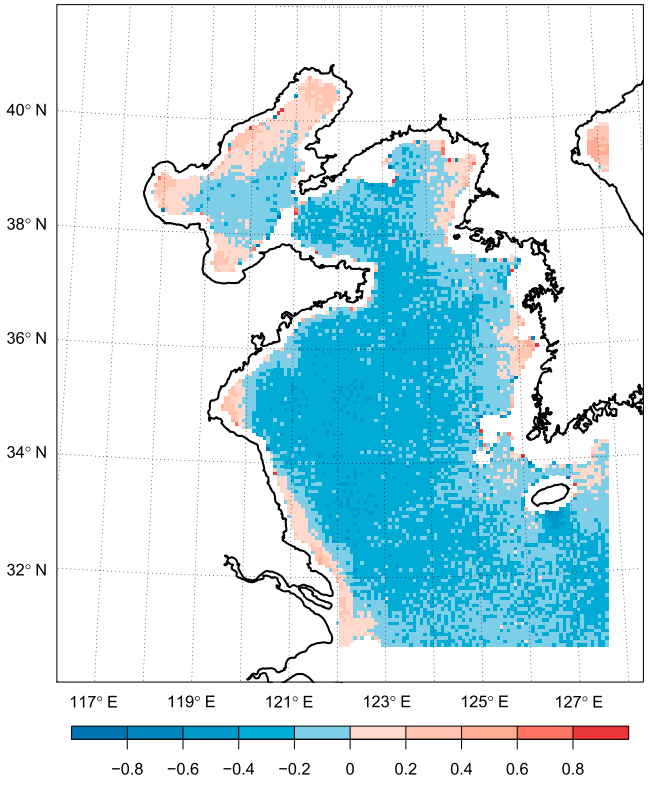

Figure 4. Brier skill score (equation (1)) distribution of CCLM relative to ERA-I with QuikSCAT as reference ("true") field.

The proportions of colocated wind speeds larger than 25 m s^{-1} are negligible, ranging between 0 and 0.2% for most areas. Figure 2b shows that the mean QuikSCAT wind speeds are approximately 7 m s^{-1} for most areas, while slightly lower mean wind speeds prevail in coastal regions and higher mean values of approximately 8 m s^{-1} are found in the southeastern part of the research domain.

The mean wind speeds of ERA-I, CCLM, and their differences from mean wind speeds of QuikSCAT are shown in Figure 3. The mean wind patterns of ERA-I and CCLM are similar to that of QuikSCAT (Figure 2b), with generally slightly lower values along coastal areas and higher values in the southeastern part of the research domain. ERA-I and CCLM underestimate the mean wind speeds for the entire domain when compared with QuikSCAT, with a 0.5 to 1 m s^{-1} underestimation in the central YS by both ERA-I and CCLM. For the whole BS, the coastal area of the YS, and the area around Jeju Island (JI), ERA-I underestimates QuikSCAT winds, with values ranging from 0.5 to 2.5 m s^{-1}; this bias is reduced by CCLM, with values of 0.1 to 0.5 m s^{-1} in the area around JI and up to 1.2 m s^{-1} in the coastal areas of BYS. CCLM performs better than ERA-I in terms of mean wind speeds in coastal and island areas with complex surroundings and orography.

To assess the improvement from dynamical downscaling using CCLM, the BSS is calculated (Figure 4). The positive BSS values indicate that added value is distributed along the coastal areas of the BYS and east to JI. On the other hand, there is no added value in the offshore area, as indicated by negative BSS values. The result shown here is consistent with the bias metrics shown in Figures 3c and 3d as well as with the results of *Sotillo et al.* [2005] and *Winterfeldt et al.* [2011] in the Mediterranean Sea and the European water area, respectively.

Additionally, comparisons of CCLM and ERA-I against some coastal and offshore station observations have been conducted (Figures 5 and 6). According to the statistical measures for coastal results (Figure 5), the absolute biases are largely reduced by CCLM when compared with ERA-I, especially for station FLA, with bias reductions up to 1.2 m s^{-1}. The RMSEs of approximately 2.0 m s^{-1} (except for FLA with 3 m s^{-1}) are generally reduced in the CCLM results. CCLM is also characterized with better reproduction of wind variability (standard deviation) than ERA-I. Based on the scatter plots, qq plots, and Kernel density estimation contours, the CCLM consistently has a better representation of coastal wind speed observations than ERA-I, especially for station SEO. In addition, for stations FLA and SEO, the improvement in wind speed distributions by CCLM tends to be more pronounced with strong winds than with light winds. In summary, CCLM fits the coastal observations closely and is much improved relative to ERA-I, especially for the strong wind speeds at coastal stations.

Figure 6 shows the same results as Figure 5 but for offshore stations. According to the given statistical measures and plots, we do not observe improvement by CCLM relative to ERA-I. Bias, RMSE, and SD for station M01 and bias for station M02 of CCLM are slightly better than those of ERA-I, whereas for the other measures, CCLM does not show any improvement relative to ERA-I. The wind speed frequency distributions between CCLM and ERA-I are similar for all three offshore stations.

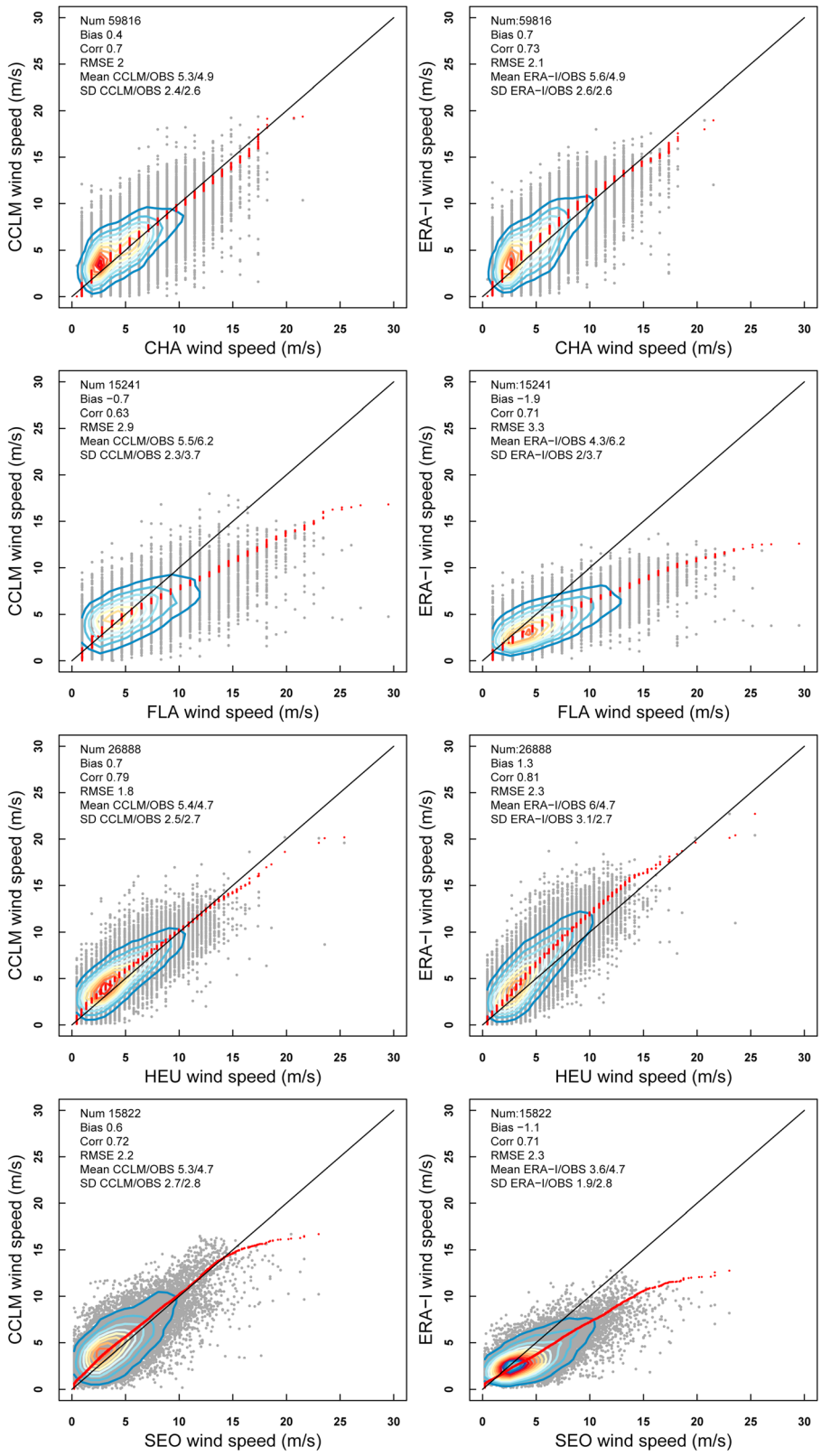

Figure 5. (left column) Comparison of CCLM (*y* axis) and (right column) ERA-I (*y* axis) with four coastal station (CHA, FLA, HEU, and SEO) wind observations (*x* axis): scatter plots (grey dots), qq plots (red dots), and several statistical measures (valid numbers of observations, bias, correlation (Corr), root-mean-square error (RMSE), mean and standard deviation (SD)). The kernel density estimations (contour lines) are included.

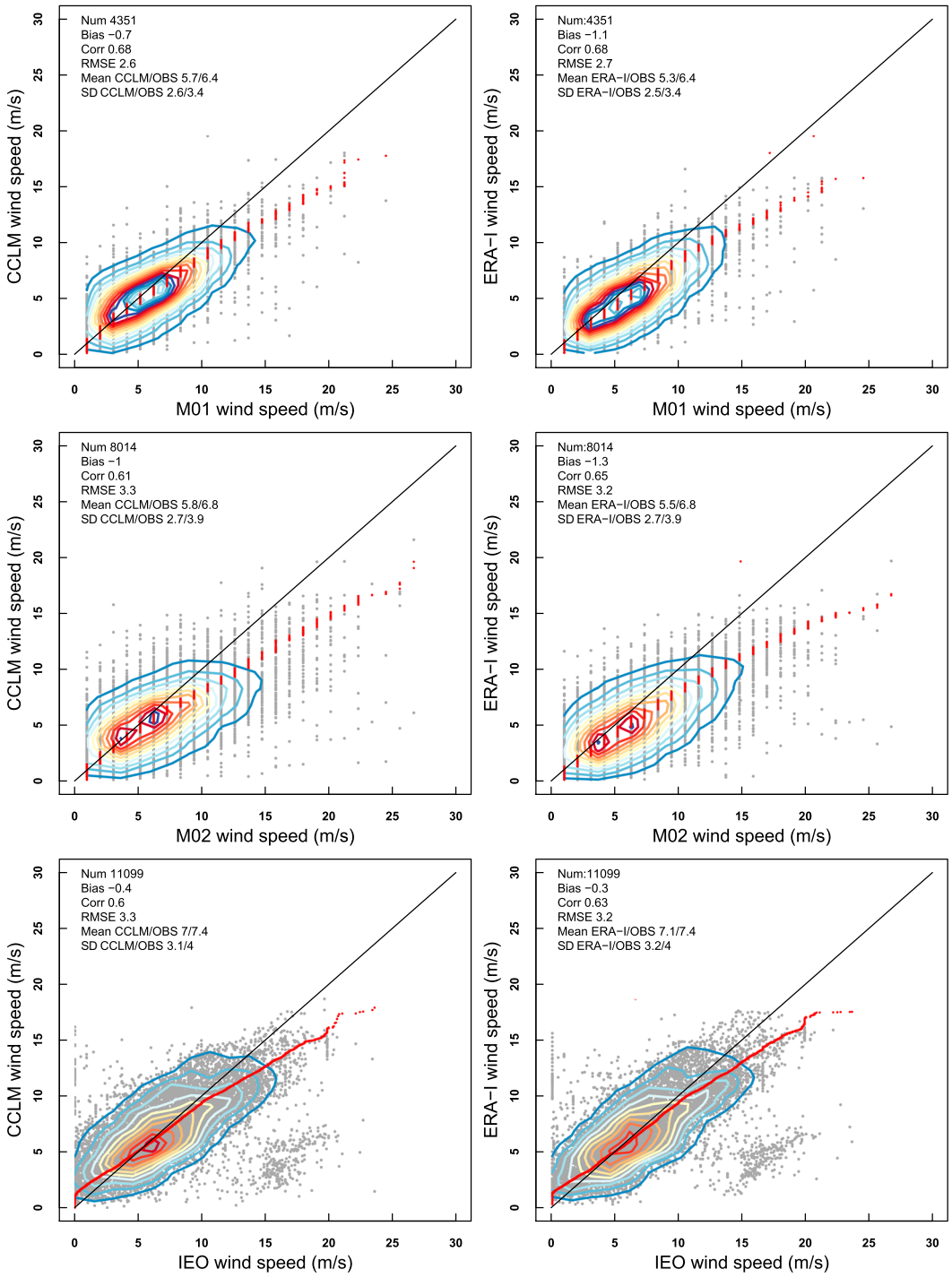

Figure 6. Same as Figure 5 but for three offshore stations (M01, M02, and IEO).

In summary, CCLM provides a realistic representation of wind speeds, and it tends to provide considerable improvements relative to the forcing data set ERA-I in coastal areas. In offshore areas, we cannot detect improvement by CCLM.

3.2. Assessment of CCLM in Reproducing Different Wind Intensities

To assess the ability of CCLM to represent different wind intensities, three classes of QuikSCAT wind speeds are clarified, with light winds at 3.0 to 5.5 m s^{-1}, moderate winds at 5.5 to 10.8 m s^{-1}, and strong winds

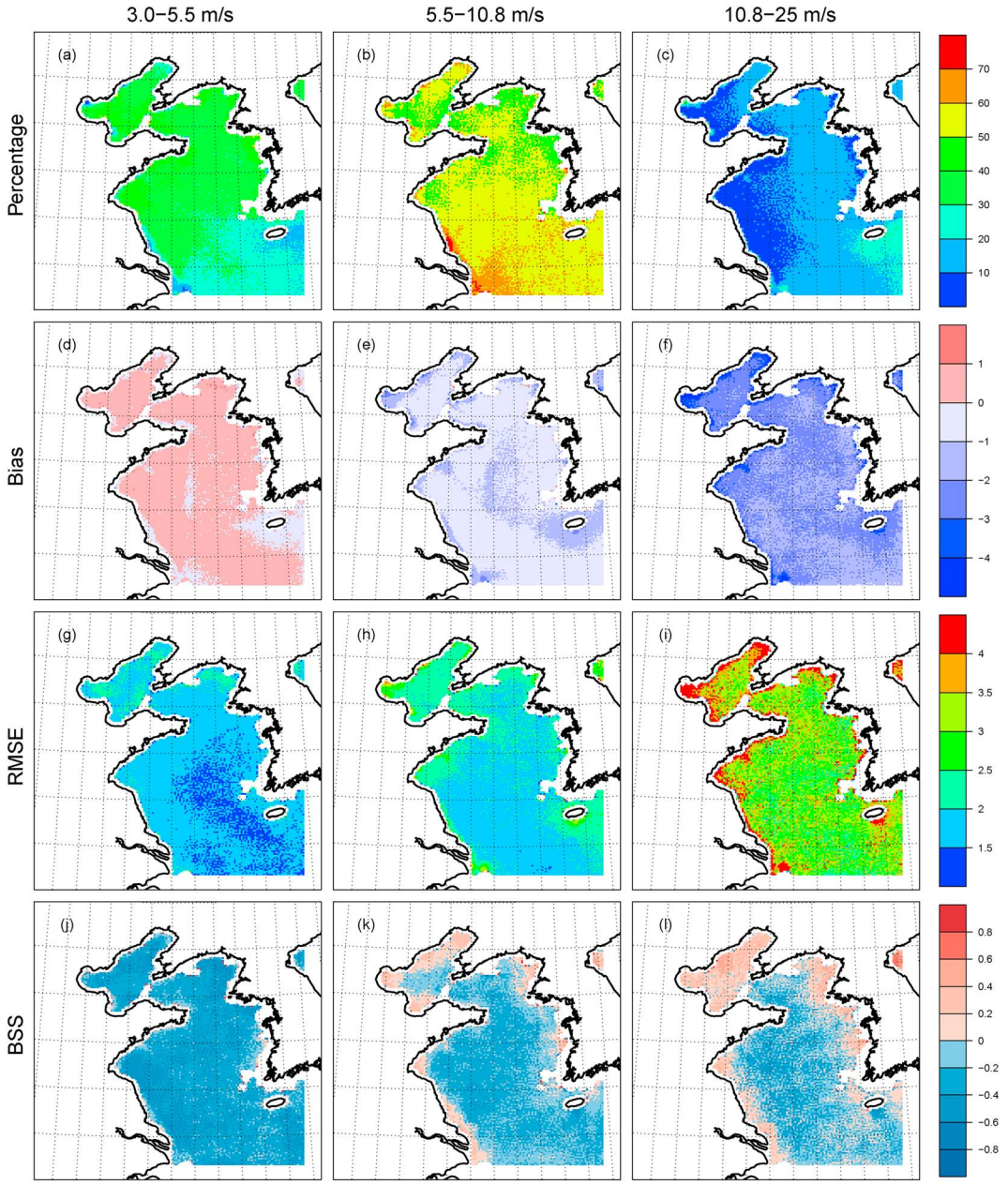

Figure 7. Measures for different wind intensities ((a, d, g, and j) 3.0–5.5 m s^{-1}, (b, e, h, and k) 5.5–10.8 m s^{-1}, (c, f, i, and l) 10.8–25 m s^{-1}): (Figures 7a–7c) the percentage of each wind intensity in the valid colocation number of QuikSCAT (3.0–25 m s^{-1}), (Figures 7d–7f) mean bias distributions of colocated CCLM and QuikSCAT, (Figures 7g–7i) root-mean-square error distributions of colocated CCLM and QuikSCAT, (Figures 7j–7l) Brier skill score distributions of CCLM relative to ERA-I with QuikSCAT as a reference ("true") field.

greater than 10.8 m s^{-1}. The spatial distribution of measures, including the proportion of all data within 3 to 25 m s^{-1}, bias, RMSE, and BSS, are used in the statistical analysis and are shown in Figure 7.

A total of 40% of all valid observations are light wind speeds (Figures 7a, 7d, 7g, and 7j), with fewer than 30% in the southeastern part of the research domain. The bias is within ±1.0 m s^{-1} for the whole area, and in most points, CCLM overestimates the observed values. The RMSE values are generally less than 2.0 m s^{-1}, with values larger than 2.0 m s^{-1} in some areas of BS and the northern YS coast. The BSS values are less than zero for nearly all regions, which indicates that CCLM does not add value to the light wind speeds relative to ERA-I.

The moderate winds (Figures 7b, 7e, 7h, and 7k) are dominant, accounting for 50% to 60% of all valid observations in most areas. The proportion is less than 50% over parts of the BS and along the northern YS coast and is more than 60% along the southwest YS coast. The biases of CCLM moderate winds mostly range from 0 to $-1\,m\,s^{-1}$ and range from -1.0 and $-2.0\,m\,s^{-1}$ in some areas along the coast and around islands (Figure 7e). The RMSE values are generally less than $2.0\,m\,s^{-1}$, but they are larger than $2.0\,m\,s^{-1}$ in the BS and coastal YS areas. The BSS distribution is similar to the one shown in Figure 4, in which added value is indicated by positive BSS along the coasts, while no added value is found in the offshore areas.

For strong wind speeds (Figures 7c, 7f, 7i, and 7l), percentages generally range from 10% to 20% but are less than 10% in parts of the BS area and the southwestern part of the YS, and are more than 20% in the southeastern part of the domain. The strong wind speeds are underestimated by CCLM by 1.0–$3.0\,m\,s^{-1}$, and the RMSE values are larger than $2.5\,m\,s^{-1}$ in most areas. Even larger RMSE values ($>3.5\,m\,s^{-1}$) are distributed along the coasts. The BSS (Figure 7l) points to added value in the entire BS and coastal YS areas. There is no indication of added value in the offshore YS areas.

Overall, CCLM performs better in terms of bias and RMSE for light and moderate wind speeds than for strong winds. Light wind speeds are overestimated by CCLM, and strong winds are underestimated. In terms of added value (as indicated by BSS; Figures 7j–7l), CCLM tend to have more improvement over the driving ERA-I data set for strong winds than for light and moderate winds, and the added value is mostly generated over the coastal areas of BYS, rather than the offshore areas. However, we need to be aware that the light winds we have considered here only include the 3.0 to $5.5\,m\,s^{-1}$ range.

3.3. Seasonality Assessment of CCLM Winds

We subsample the co-located data into the four seasons, winter (December–February, DJF), spring (March–May, MAM), summer (June–August, JJA), and autumn (September–November, SON), to assess the seasonal performance of CCLM in reproducing wind speeds. Figure 8 shows the distribution of the statistical measures of CCLM compared with the QuikSCAT data. Figures 8a–8d indicate that CCLM tends to underestimate wind speeds in winter and autumn by approximately $1.0\,m\,s^{-1}$ and to overestimate winds in some areas in spring and summer. The overestimation in spring is in the BS and northern YS areas as well as the southern coastal YS areas and is mainly along the coastal BYS areas in summer. Furthermore, the seasonal area-averaged wind speeds of CCLM, ERA-I, and QuikSCAT as well as their spatial standard deviations (Figure 9) indicate an underestimation by CCLM and ERA-I for all seasons. However, CCLM has improvements in spring, summer, and autumn relative to ERA-I, especially for the summer season, with considerable bias reduction.

Correlations between CCLM and QuikSCAT winds are much higher in winter and autumn than in spring and summer (Figures 8e–8g). During winter and autumn, the correlations are approximately 0.85, but up to 0.90 in some areas, and are generally more than 0.70 in the coastal area. During spring, the values are mostly larger than 0.70, with values of approximately 0.60 in the coastal areas; however, in summer, correlations are approximately 0.70 in most areas and lower than 0.60 in some coastal areas. The RMSE has values of app. $2.0\,m\,s^{-1}$ in offshores areas and somewhat larger values of approximately $2.5\,m\,s^{-1}$ or more in coastal or island areas. Seasonal differences are small, except for summer, which has relatively larger RMSE values. According to the BSS during winter and spring (Figures 8m and 8n), added value is present in coastal areas but not in offshore areas. Figures 8o and 8p show that there are more coastal areas with added value in summer and autumn than in winter and spring. In summer, there are indications for added value even in parts of the offshore areas.

In summary, we can see that CCLM has good agreement with observations in different seasons; however, the performance of CCLM varies strongly from season to season, especially between summer and the other seasons. CCLM tends to have poorer performance in reproducing winds in summer than in the other three seasons in terms of correlation and RMSE; however, when considering bias and BSS, CCLM offers improvements relative to ERA-I in summer. The assessment scores based on station-observed data are consistent with those based on QuikSCAT data. The minor differences between them are inevitable given the different temporal and spatial coverage (not shown here).

3.4. Added Value of Wind Variability of Different Scales

Global reanalyses or global climate simulations are more realistic in terms of large-scale dynamics, while the RCMs are expected to be better in resolving medium-scale phenomena [*von Storch*, 1999;

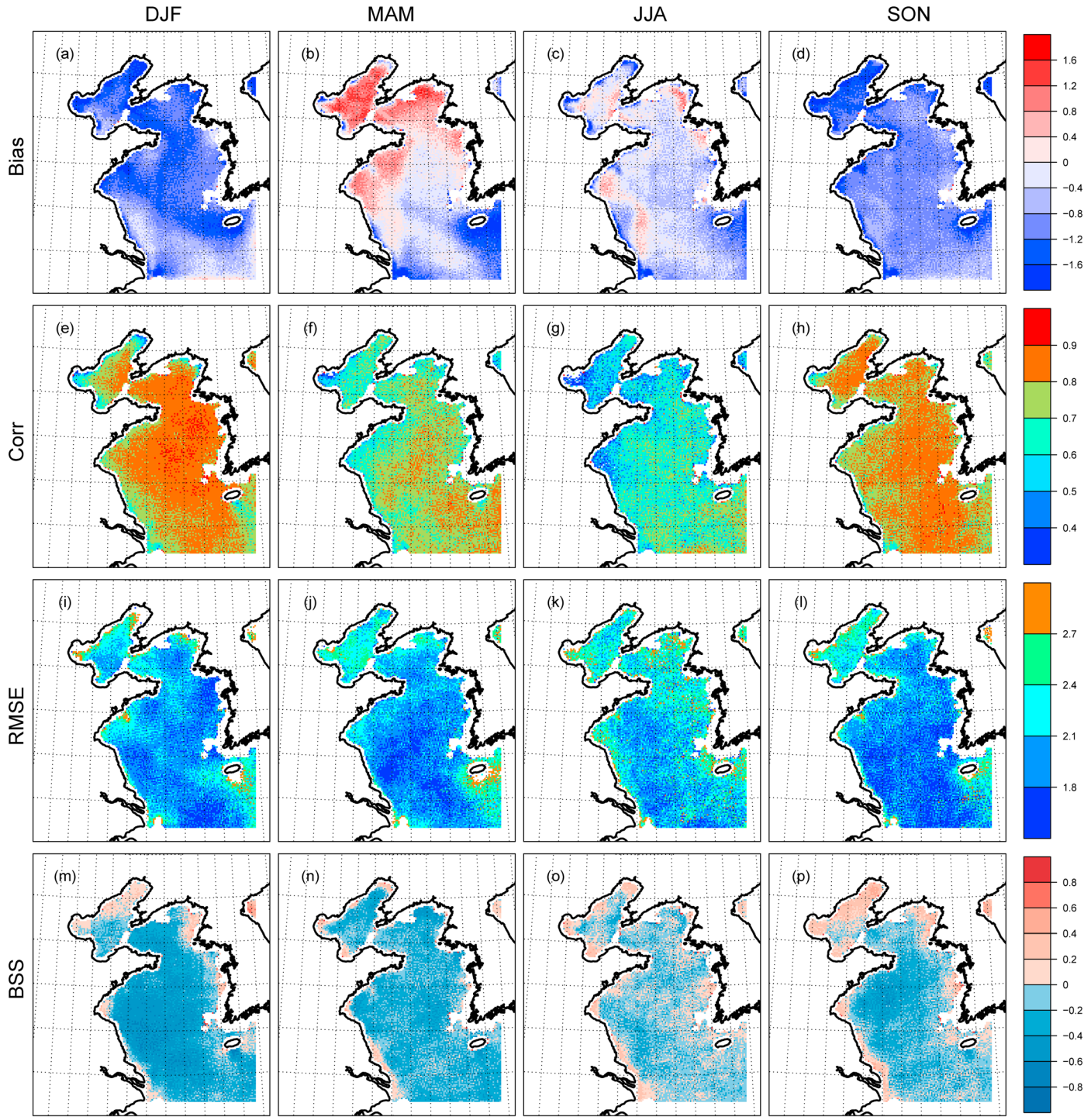

Figure 8. Seasonal statistical measures of CCLM compared with QuikSCAT data: (a–d) mean bias (m s^{-1}), (e–h) correlation coefficients, (i–l) root-mean-square error (m s^{-1}), and (m–p) Brier skill score.

Hong and Kanamitsu, 2014; *Xue et al.,* 2014]. To clearly distinguish the scale-dependent added value by CCLM, a scale separation is necessary.

Here we use a spatial digital filter [*Feser and von Storch*, 2005] to perform the scale separation. The two-dimensional isotropic discrete filters with footprints of 21×21 grid points are constructed to determine the scale-dependent components of two-dimensional fields. The setup of grid number of footprints aims

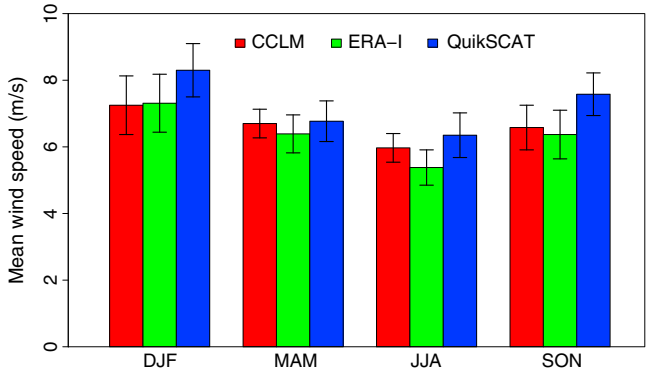

Figure 9. Barplots of area-averaged seasonal mean wind speeds by CCLM, ERA-I, and QuikSCAT (3–25 m/s). The error bars indicate the spatial standard deviations.

to get rid of the effect of sponge zone on filtered results [cf. *Feser and von Storch*, 2005]. We consider a large-scale (low-pass) and a medium-scale (band-pass) component of the surface wind speeds.

The filter parameters are optimized using the method of *Feser and von Storch* [2005]. For the low-pass filter, the retained (relative to the considered region) wavenumber range is 0 to 4, meaning that features larger than 300 km (which are supposedly well resolved by ERA-I) can pass this

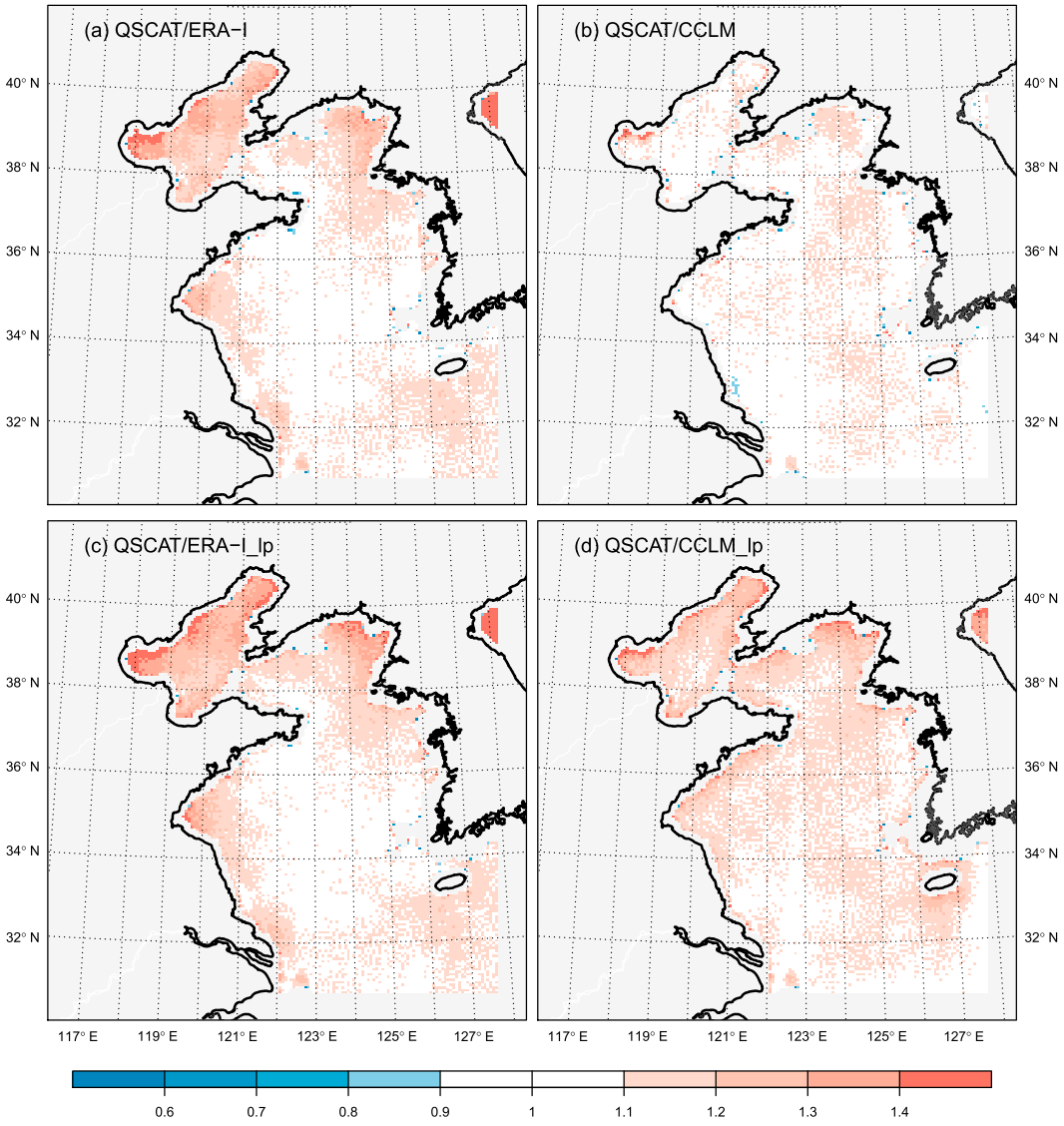

Figure 10. Standard deviation ratio distribution of QuikSCAT grid data to those of (a) ERA-I, (b) CCLM, (c) low-pass ERA-I (ERA-I_lp), and (d) low-pass CCLM (CCLM_lp). The land and sponge boundary areas are indicated in grey.

Table 2. Area-Averaged Standard Deviation (SD) of Complete Colocation Data Sets QuikSCAT (Q), ERA-I (E) and CCLM (C), Low-Pass Filtered (SD_lp), and Band-Pass Filtered (SD_bp) CCLM, and ERA-I in the Colocation Period (All) and for the Four Seasons

	All			DJF			MAM			JJA			SON		
	SD	SD_lp	SD_bp	SD	SD_lp	SD_bp	SD	SD_lp	SD_bp	SD	SD_lp	SD_bp	SD	SD_lp	SD_bp
Q	2.89			3.0			2.68			2.45			2.83		
E	2.61	2.58	0.60	2.71	2.68	0.62	2.44	2.42	0.56	2.19	2.15	0.51	2.58	2.55	0.60
C	2.71	2.58	0.82	2.74	2.63	0.78	2.52	2.39	0.78	2.48	2.33	0.80	2.74	2.61	0.81

filter. The retained relative wave number range of our medium-pass filter is set at 8 to 18, which retains phenomena with scales ranging from 65 to 150 km. However, it is important to note that the response function of a digital filter is smooth, which means that the filtered scales are not sharply truncated. For example, in the case of medium-scale features, the large- or small-scale features are not completely but only mostly removed. Furthermore, the spatial digital filter is performed only on the ERA-I and CCLM wind fields. Because of the sparse temporal and spatial coverage of QuikSCAT, a scale separation is not possible for this data set. The filtered ERA-I and CCLM wind fields are then temporally and spatially masked based on the availability of QuikSCAT data. The assessment of scale-dependent added value is based on the ratio of standard deviation, as indicated in Figure 10.

Figures 10a and 10b show the ratio of standard deviations of QuikSCAT grid data to ERA-I and CCLM. As we can see, a large part of BYS in Figure 10a is characterized by ratios larger than 1.1, which means that the QuikSCAT data have higher variability than those of ERA-I. However, in Figure 10b, a much higher agreement between CCLM and QuikSCAT data has been found, as most areas have ratios ranging from 0.9 to 1.1. Most of the improvement is over the BS and coastal areas of the YS. Therefore, we can say that added values are generated by CCLM relative to ERA-I in terms of wind variability, which is consistent with the results of previous sections.

After the low-pass spatial filter is applied to ERA-I and CCLM, we find various levels of change for the ERA-I group (Figures 10a and 10c) and the CCLM group (Figures 10b and 10d). The general patterns of ratios shown in Figures 10a and 10c are similar and are characterized by small differences. This result means that the low-pass filtered ERA-I is almost consistent with the ERA-I full wind field in wind variability, indicating that ERA-I can well represent relatively large-scale features but barely represent medium- or small-scale features. In terms of the CCLM group, however, we see worse metric values (Figure 10d) than the ones shown in Figure 10b, which indicates that the CCLM full field can represent wind variability with better skills than the low-pass filtered CCLM field. For this reason, we conclude that CCLM has added value in medium- or small-scale features in terms of wind variability relative to ERA-I.

In Table 2, we summarize the area-averaged standard deviations (SD) of the complete co-location fields of QuikSCAT, CCLM, and ERA-I, as well as low-pass filtered (SD_lp) and band-pass filtered (SD_bp) CCLM and ERA-I for the entire period and for the four seasons. In terms of standard deviation, we can see that the values of CCLM are much closer to QuikSCAT than those of ERA-I, especially during summer and autumn seasons. For SD_lp, we see the values are consistent between ERA-I and CCLM, with some differences in summer and autumn, indicating the general consistency of the large scale represented by ERA-I and CCLM. When considering SD_bp, we see the values of CCLM are much larger than those of ERA-I.

Therefore, we can conclude that wind variability can be better represented by CCLM than by ERA-I when compared with QuikSCAT, and the improvement is mainly due to the medium-scale features. The results herein are reasonable as the large scale of CCLM is spectrally nudged to the one of ERA-I, however, CCLM is free to develop fine-scale features without the limitations of ERA-I.

4. Analysis of Sea Surface Wind Climatologies

The evaluation undertaken in the previous sections revealed that the sea surface wind over the BYS is well represented by the CCLM hindcast driven by ERA-I. The hindcast, with high resolution in temporal and spatial scales as well as a long-term period (1979–2012), is an ideal source to analyse the wind climatology in our study domain.

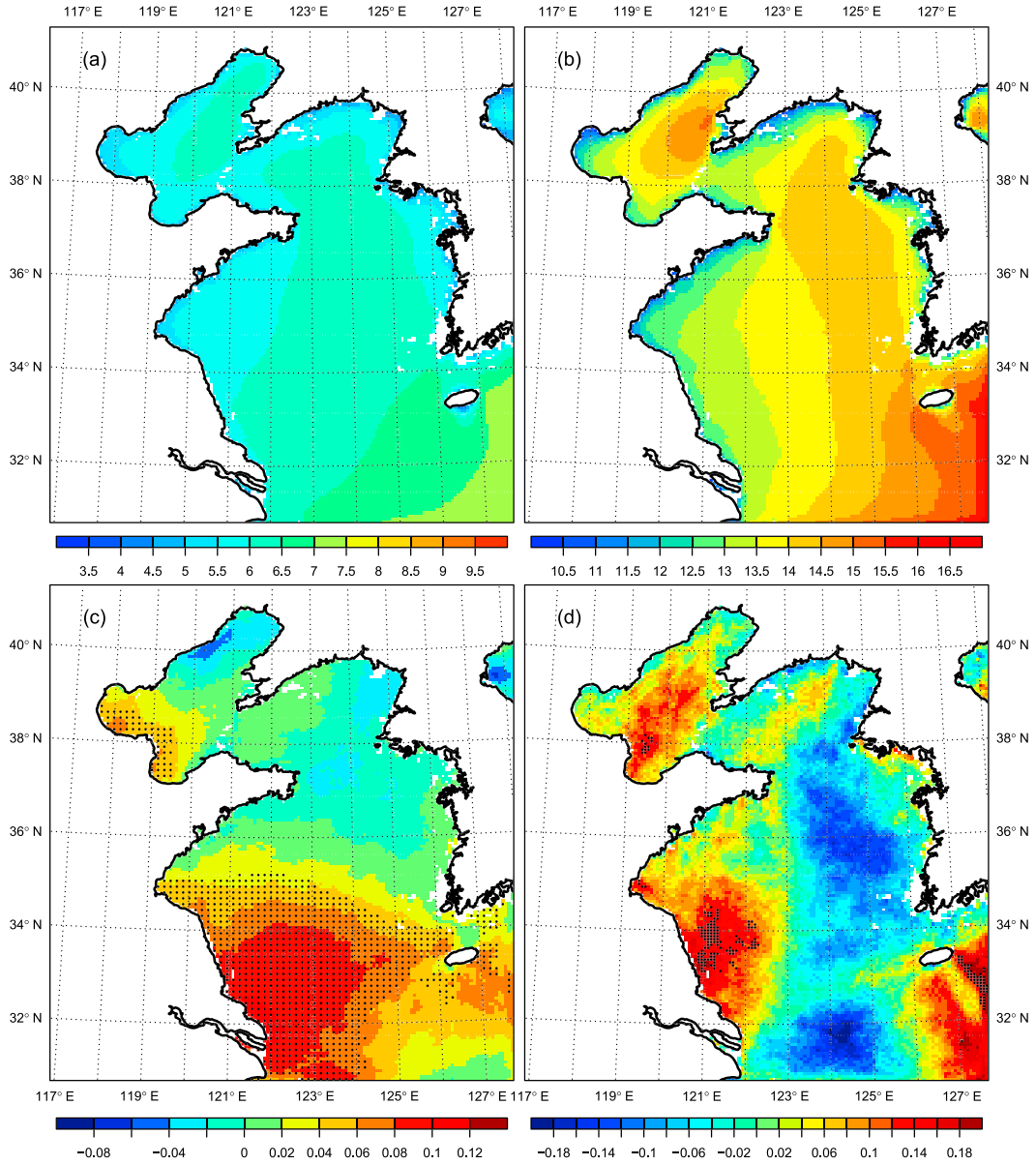

Figure 11. CCLM wind climatology from 1979 to 2012: (a) annual mean wind speeds (m s^{-1}), (b) mean annual 99th percentile wind speeds (m s^{-1}), (c) linear trends of Figure 11a with unit m s^{-1} decade^{-1}, the black dotted areas are at a 0.05 significance level, and (d) the same as Figure 11c but for linear trends of Figure 11b.

Figure 11 shows the mean wind speeds, the mean annual 99th percentile wind speeds, and their linear trends from 1979 to 2012. The mean wind speeds range in space from 4.0 m s^{-1} to 7.5 m s^{-1}, with low values along the coasts and relatively larger values in the offshore areas. The mean wind speeds increase from north to south and have the largest values in the southeastern part of our study domain (Figure 11a). The distribution is very similar to the field derived from the QuikSCAT-related subset shown in Figure 3. The characteristics of the mean annual 99th percentiles (Figure 11b) are similar to the mean field, however, the values are approximately 12.5 m s^{-1} in the coastal areas, approximately 14.5 m s^{-1} in the central BYS, and more than 15.0 m s^{-1} in the southeastern part. The mean wind speeds increase significantly in the south of YS, with a strength of 0.06 m s^{-1} decade^{-1} and more, and some areas can reach up to 0.1 m s^{-1} decade^{-1} (Figure 11c); in most areas of BS and north YS, no significant trend is detected. The trends of the mean annual 99th percentile wind speeds (Figure 11d) vary substantially in the BS and YS areas, with values between 0.18 m s^{-1} decade^{-1} and −0.18 m s^{-1} decade^{-1}; however, these trends generally did not pass the significance test at the 0.05 level.

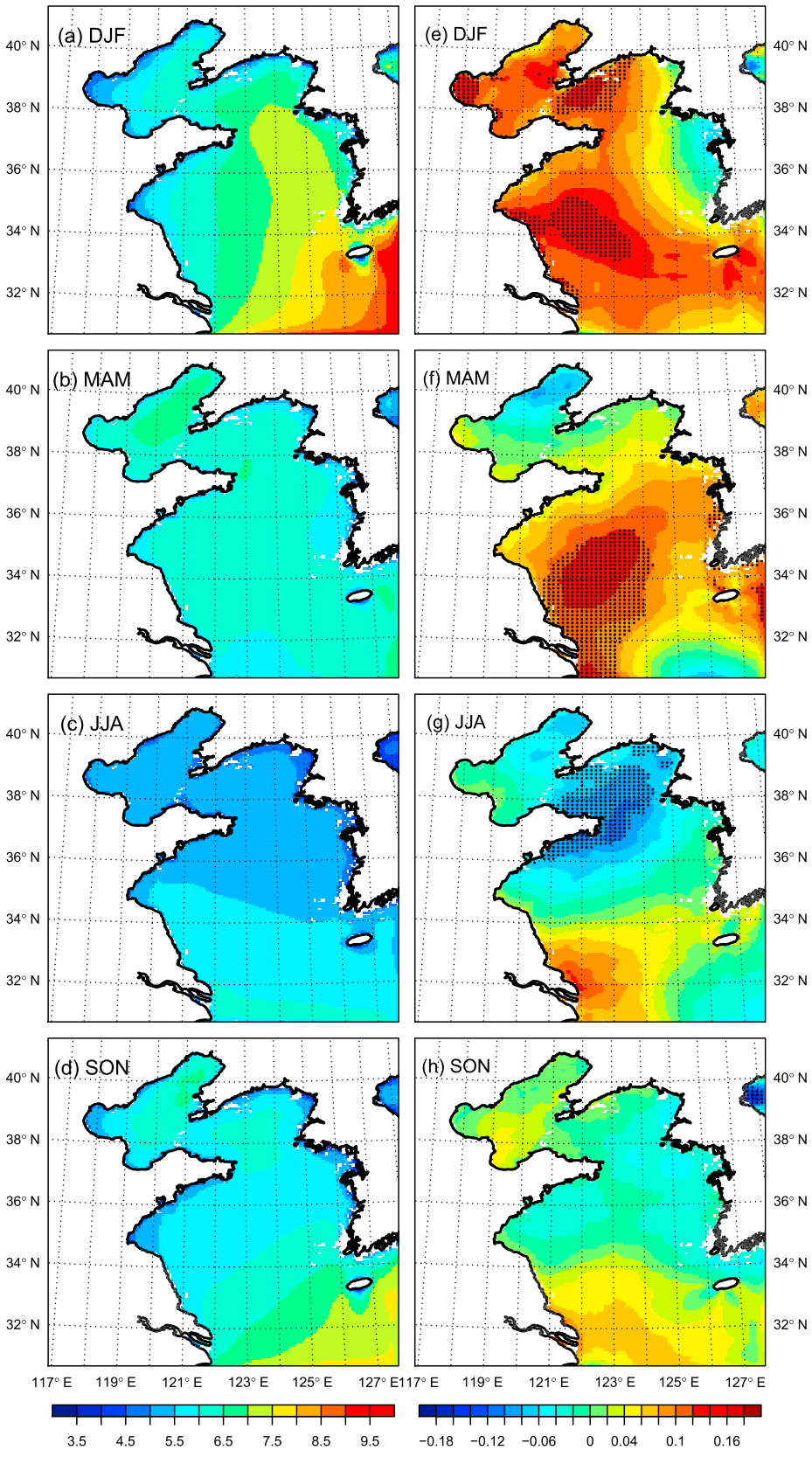

Figure 12. (a–d) CCLM seasonal mean wind speeds (m s^{-1}), (e–h) CCLM linear trend (m s^{-1} $decade^{-1}$) of seasonal mean wind speeds from 1979 to 2012, and the black dotted areas are at a 0.05 significance level.

The seasonal mean wind speeds and corresponding linear trends from 1979 to 2012 are shown in Figure 12. Low mean wind speeds are found in the coastal areas, and various spatial distributions are observed in the offshore areas. The seasonal mean wind speeds are largest in winter and smallest in summer (Figures 12a and 12c). The spatial distributions are more uniform in spring and summer (Figures 12b and 12c) than in winter and autumn (Figures 12a and 12d). In terms of the trend distribution of seasonal mean wind speeds, we find strong positive trends in winter (Figure 12e), with strength up to 0.18 m s^{-1} decade^{-1} at 0.05 significance levels. Significant positive trends in spring (Figure 12f) are mainly distributed in the southern YS, with values larger than 0.12 m s^{-1} decade^{-1}, and some weak negative trends are observed in two areas. Figure 12g shows negative trends in the northern YS and positive trends in the southwestern YS in summer, with strength larger than 0.12 m s^{-1} decade^{-1} at a 0.05 significance level. We also assess the trend of seasonal 99th percentile wind speeds (not shown here). We find strong positive trends with strength up to 0.3 m s^{-1} decade^{-1} at 0.05 significance levels in the western YS in winter as well as in southwestern and southeastern YS in spring. In summer and autumn, the trends are mainly negative in the YS and mainly positive in the BS, with strength up to 0.5 m s^{-1} decade^{-1}; however, these trends generally did not pass the significance test at the 0.05 level.

5. Discussion and Conclusions

In this study, a 34 year (1979–2012) wind hindcast with a high resolution (7 km) has been performed over the Bohai Sea and the Yellow Sea in East Asia using the regional atmospheric model CCLM driven by reanalysis data set ERA-I. The quality of the wind hindcast is first assessed by comparisons against station observations and QuikSCAT data using different statistical measures. During the assessment process, two main issues are addressed: whether CCLM and ERA-I can reproduce the real wind conditions in the BYS, including general wind characteristics, seasonal variability, and wind intensities features, and whether CCLM can add value to the description of the wind fields compared to ERA-I.

Through comparisons with QuikSCAT, we found that CCLM has reliable performance in reproducing the observed wind speeds and can produce improvements relative to ERA-I, especially in coastal areas with complex orography, whereas there is no added value in the offshore areas of the open sea.

The assessment of the performance of CCLM at different wind intensities shows that CCLM is better at representing light and moderate wind speeds than strong wind speeds; however, in regard to strong winds, CCLM generates added value for a larger area relative to ERA-I than it does for light or moderate wind speeds. Strong seasonal variability is found, and CCLM tends to have better performance in reproducing wind in spring, autumn, and winter than in summer in terms of correlation and root mean square error with QuikSCAT. With respect to bias, CCLM shows more improvement relative to ERA-I in summer than in the other three seasons. In terms of added value measured by the Brier skill score, we see CCLM primarily adding value in the coastal areas in all seasons, as expected; however, larger areas of added value can be detected in summer and autumn than in winter and spring.

The result, i.e., added value is generated in the coastal water areas rather than in offshore areas, confirms previous findings over European water areas by *Sotillo et al.* [2005] and *Winterfeldt et al.* [2011]. As revealed by section 3.4 using the spatial filter method, the added value is highly related to the better representation of medium-scale features by CCLM. These analyses focus on the quantitative analysis of the total added value by RCM, but some physical processes underlying this statistical added value have not been investigated. The medium-scale processes in the coastal areas of BYS, including flow blocking, sea-land fronts, vortex street, and mountain gap winds [*Wang*, 2006; *Chung and Kim*, 2008; *Liang et al.,* 2013], are highly related to local orography, which may be dominant factors that contribute to the added value of CCLM in coastal and island areas. Mesoscale convective systems and low level jets are widely distributed in our research domain, especially during summer [*Chen et al.,* 1999; *Li et al.,* 2012; *Du et al.,* 2014], which increases the potential of added value in the summer compared to other seasons. Additionally, the weather system is highly affected by some synoptic or sub-synoptic systems, such as tropical cyclones (TCs). We found that some strong or extreme wind cases are related to TCs and are better reproduced by CCLM than by ERA-I, especially in terms of wind intensities (not shown here), which may be another potential factor involved in added value. However, in this study, we mainly focus on the total added value using statistical metric scores. The underlying physical processes that contribute to total added value compared to the forcing data set ERA-I by CCLM will be investigated in the future in more detail.

Additionally, the annual, seasonal, and extreme wind climatologies, as well as the corresponding trend distributions, have been briefly investigated in this paper. The trend analysis of the mean wind speeds reveals strong spatial and seasonal variations, with significant increases in the southern YS, with trends generally larger than 0.06 m s^{-1} $decade^{-1}$, which is consistent with the wind trend map computed by *Wentz et al.* [2007] using satellite observations from 1987 to 2006. These trends in the southern YS are much stronger in winter and spring, with values of more than 0.12 m s^{-1} $decade^{-1}$. *Oey et al.* [2013] also revealed an increasing trend of northeasterly winds in winter on the eastern coast of China and related this increase with the warming of Chinese shelf seas within a positive feedback triggered by the El Nino in 1997–1998.

In summary, the high-resolution model-reconstructed wind data set proves to be robust in reproducing the surface wind conditions over the BYS over recent decades (1979–2012), and it can add value to the driving data set. The data set can be widely used in coastal and offshore applications, such as the building code of oil platform, which are significantly affected by wind conditions, especially by extreme wind events. Offshore wind energy assessments have been conducted based on the data set, which is a reference for wind farm constructions. This data set can also be used as forcing for others, such as wave and storm surge simulations, which can contribute greatly to a comprehensive assessment of the marine climate over the BYS.

Acknowledgments

The authors thank the two anonymous reviewers for their helpful comments. The authors would like to thank the China Scholarship Council (CSC201206330070) and the REKLIM project (LK14401KSG0101) for their financial support. We thank B. Rockel, F. Feser, and T. Frisius for their valuable discussions. The following institutions, which provided the data, are acknowledged: the QuikSCAT obtained freely from the Physical Oceanography Distributed Active Archive Center (PO. DAAC) at the NASA Jet Propulsion Laboratory (ftp://podaac-ftp.jpl.nasa.gov/allData/quikscat/L2B12/v3/), observation data available freely at the National Climate Data Center (NCDC, ftp://ftp.ncdc.noaa.gov/pub/data/noaa/) and at the National Marine Data and Information Service of China (NMDIS, http://www.odinwestpac.org.cn/finddata.aspx), the reanalysis data set ERA-I obtained from the European Centre for Medium-Range Weather Forecasts (ECMWF, http://apps.ecmwf.int/datasets/data/interim-full-daily) following registration, and the model external forcing data obtained freely from the Climate Limited-area Modelling-Community. (http://www.clm-community.eu/index.php?menuid=221). We also acknowledge the German Climate Computing Center (DKRZ) for providing the computational facilities for our simulation.

References

Aguilar, E., I. Auer, M. Brunet, T. C. Peterson, and J. Wieringa (2003), Guidance on metadata and homogenization, *WMO TD 1186*, 53 pp.

Alvarez, I., M. Gomez-Gesteira, M. deCastro, and D. Carvalho (2013), Comparison of different wind products and buoy wind data with seasonality and interannual climate variability in the southern Bay of Biscay (2000–2009), *Deep Sea Res., Part II*, *106*, 38–48, doi:10.1016/j.dsr2.2013.09.028.

Bentamy, A., S. A. Grodsky, J. A. Carton, D. Croizé-Fillon, and B. Chapron (2012), Matching ASCAT and QuikSCAT winds, *J. Geophys. Res.*, *117*, C02011, doi:10.1029/2011JC007479.

Blain, G. C. (2013), The Mann-Kendall test: The need to consider the interaction between serial correlation and trend, *Acta Sci. Agron.*, *35*(4), 393–402.

Chen, S.-J., D.-K. Lee, Z.-Y. Tao, and Y.-H. Kuo (1999), Mesoscale convective system over the Yellow Sea—A numerical case study, *Meteorol. Atmos. Phys.*, *70*(3–4), 185–199.

Chung, Y. S., and H. S. Kim (2008), Mountain-generated vortex streets over the Korea South Sea, *Int. J. Remote Sens.*, *29*(3), 867–877, doi:10.1080/01431160701281080.

Dee, D., et al. (2011), The ERA-Interim reanalysis: Configuration and performance of the data assimilation system, *Q. J. R. Meteorol. Soc.*, *137*(656), 553–597, doi:10.1002/qj.828.

Dee, D., J. Fasullo, D. Shea, J. Walsh, and National Center for Atmospheric Research Staff (2014), The climate data guide: Atmospheric reanalysis: Overview & comparison table. [Available at https://climatedataguide.ucar.edu/climate-data/atmospheric-reanalysis-overview-comparison-tables.]

Di Luca, A., R. de Elía, and R. Laprise (2015), Challenges in the quest for added value of regional climate dynamical downscaling, *Curr. Clim. Change Rep.*, *1*(1), 10–21, doi:10.1007/s40641-015-0003-9.

Du, Y., Q. Zhang, Y. Chen, Y. Zhao, and X. Wang (2014), Numerical simulations of spatial distributions and diurnal variations of low-level jets in China during early summer, *J. Clim.*, *27*(15), 5747–5767, doi:10.1175/jcli-d-13-00571.1.

Feldmann, H., B. Frueh, G. Schaedler, H.-J. Panitz, K. Keuler, D. Jacob, and P. Lorenz (2008), Evaluation of the precipitation for South-western Germany from high resolution simulations with regional climate models, *Meteorol. Z.*, *17*(4), 455–465, doi:10.1127/0941-2948/2008/0295.

Feser, F., and H. von Storch (2005), A spatial two-dimensional discrete filter for limited-area-model evaluation purposes, *Mon. Weather Rev.*, *133*(6), 1774–1786, doi:10.1175/mwr2939.1.

Feser, F., and H. von Storch (2008), A dynamical downscaling case study for typhoons in Southeast Asia using a regional climate model, *Mon. Weather Rev.*, *136*(5), 1806–1815, doi:10.1175/2007mwr2207.1.

Fore, A. G., B. W. Stiles, A. H. Chau, B. A. Williams, R. S. Dunbar, and E. Rodríguez (2014), Point-wise wind retrieval and ambiguity removal improvements for the QuikSCAT climatological data set, *IEEE Trans. Geosci. Remote Sens.*, *52*(1), 51–59, doi:10.1109/TGRS.2012.2235843.

Geyer, B. (2014), High-resolution atmospheric reconstruction for Europe 1948-2012: CoastDat2, *Earth Syst. Sci. Data*, *6*(1), 147–164, doi:10.5194/essd-6-147-2014.

Hoffman, R. N., and S. M. Leidner (2005), An introduction to the near-real-time QuikSCAT data, *Weather Forecasting*, *20*(4), 476–493, doi:10.1175/WAF841.1.

Hong, S.-Y., and M. Kanamitsu (2014), Dynamical downscaling: Fundamental issues from an NWP point of view and recommendations, *Asia-Pac. J. Atmos. Sci.*, *50*(1), 83–104, doi:10.1007/s13143-014-0029-2.

Jiménez, P. A., J. F. González-Rouco, E. García-Bustamante, J. Navarro, J. P. Montávez, J. V.-G. de Arellano, J. Dudhia, and A. Muñoz-Roldan (2010), Surface wind regionalization over complex terrain: Evaluation and analysis of a high-resolution WRF simulation, *J. Appl. Meteorol. Climatol.*, *49*(2), 268–287, doi:10.1175/2009JAMC2175.1.

Kalnay, E., et al. (1996), The NCEP/NCAR 40-year reanalysis project, *Bull. Am. Meteorol. Soc.*, *77*(3), 437–471.

Kara, A. B., A. J. Wallcraft, P. J. Martin, and R. L. Pauley (2009), Optimizing surface winds using QuikSCAT measurements in the Mediterranean Sea during 2000-2006, *J. Mar. Syst.*, *78*, 119–131, doi:10.1016/j.jmarsys.2009.01.020.

Kendall, M. G. (1948), *Rank Correlation Methods*, Charles Griffin, London.

Kessler, E. (1969), On the distribution and continuity of water substance in atmospheric circulations, *Meteorol. Monogr.*, *32*(10), 18–54.

Kobayashi, S., et al. (2015), The JRA-55 reanalysis: General specifications and basic characteristics, *J. Meteorol. Soc. Jpn.*, *93*(1), 5–48, doi:10.2151/jmsj.2015-001.

Lee, D.-K., D.-H. Cha, C.-S. Jin, and S.-J. Choi (2013), A regional climate change simulation over East Asia, *Asia-Pac. J. Atmos. Sci.*, *49*(5), 655–664, doi:10.1007/s13143-013-0058-2.

Lee, J.-W., and S.-Y. Hong (2014), Potential for added value to downscaled climate extremes over Korea by increased resolution of a regional climate model, *Theor. Appl. Climatol.*, *117*(3–4), 667–677, doi:10.1007/s00704-013-1034-6.

Lee, J.-W., S.-Y. Hong, E.-C. Chang, M.-S. Suh, and H.-S. Kang (2014), Assessment of future climate change over East Asia due to the RCP scenarios downscaled by GRIMs-RMP, *Clim. Dyn.*, *42*(3–4), 733–747, doi:10.1007/s00382-013-1841-6.

Li, D., H. von Storch, and B. Geyer (2015), Testing reanalyses in constraining dynamical downscaling, *J. Meteorol. Soc. Jpn.*, doi:10.2151/jmsj.2015-044.

Li, J., B. Wang, and D.-H. Wang (2012), The characteristics of Mesoscale Convective Systems (MCSs) over East Asia in warm seasons, *Atmos. Oceanic Sci. Lett.*, *5*(2), 102–107.

Liang, Z., S.-T. Gao, and Y. Wang (2013), Data analysis of collision-type sea-breeze front in the Bohai Bay Region, *Clim. Environ. Res.*, *18*(5), 607–616, doi:10.3878/j.issn.1006-9585.2012.12002.

Mann, H. B. (1945), Nonparametric tests against trend, *Econometrica*, *13*, 245–259.

Menendez, M., M. García-Díez, L. Fita, J. Fernández, F. Méndez, and J. M. Gutiérrez (2013), High-resolution sea wind hindcasts over the Mediterranean area, *Clim. Dyn.*, *42*(7–8), 1857–1872, doi:10.1007/s00382-013-1912-8.

Moroni, D., B. Stiles, and A. Fore (2013), QuikSCAT Level 2B Version 3 Guide Document, pp. 1–16, NASA JPL Phys. Oceanogr. DAAC.

Oey, L.-Y., M.-C. Chang, Y.-L. Chang, Y.-C. Lin, and F.-H. Xu (2013), Decadal warming of coastal China Seas and coupling with winter monsoon and currents, *Geophys. Res. Lett.*, *40*, 6288–6292, doi:10.1002/2013gl058202.

Panitz, H.-J., A. Dosio, M. Büchner, D. Lüthi, and K. Keuler (2013), COSMO-CLM (CCLM) climate simulations over CORDEX-Africa domain: Analysis of the ERA-Interim driven simulations at 0.44° and 0.22° resolution, *Clim. Dyn.*, *42*(11–12), 3015–3038, doi:10.1007/s00382-013-1834-5.

Portoghese, I., E. Bruno, P. Dumas, N. Guyennon, S. Hallegatte, J.-C. Hourcade, H. Nassopoulos, G. Pisacane, M. V. Struglia, and M. Vurro (2013), Impacts of climate change on freshwater bodies: Quantitative aspects, in *Regional Assessment of Climate Change in the Mediterranean*, pp. 241–306, Springer, Berlin.

Pryor, S., G. Nikulin, and C. Jones (2012), Influence of spatial resolution on regional climate model derived wind climates, *J. Geophys. Res.*, *117*, D03117, doi:10.1029/2011JD016822.

Reistad, M., Ø. Breivik, H. Haakenstad, O. J. Aarnes, B. R. Furevik, and J.-R. Bidlot (2011), A high-resolution hindcast of wind and waves for the North Sea, the Norwegian Sea, and the Barents Sea, *J. Geophys. Res.*, *116*, C05019, doi:10.1029/2010JC006402.

Risien, C. M., and D. B. Chelton (2008), A global climatology of surface wind and wind stress fields from eight years of QuikSCAT scatterometer data, *J. Phys. Oceanogr.*, *38*(11), 2379–2413, doi:10.1175/2008jpo3881.1.

Ritter, B., and J.-F. Geleyn (1992), A comprehensive radiation scheme for numerical weather prediction models with potential applications in climate simulations, *Mon. Weather Rev.*, *120*(2), 303–325.

Rockel, B., A. Will, and A. Hense (2008), The Regional Climate Model COSMO-CLM (CCLM), *Meteorol. Z.*, *17*(4), 347–348, doi:10.1127/0941-2948/2008/0309.

Schrodin, R., and E. Heise (2002), A new multi-layer soil model, *COSMO Newsl.*, *2*, 149–151.

Sen, P. K. (1968), Estimates of the regression coefficient based on Kendall's tau, *J. Am. Stat. Assoc.*, *63*(324), 1379–1389.

Sotillo, M., A. Ratsimandresey, J. Carretero, A. Bentamy, F. Valero, and F. González-Rouco (2005), A high-resolution 44-year atmospheric hindcast for the Mediterranean Basin: Contribution to the regional improvement of global reanalysis, *Clim. Dyn.*, *25*(2–3), 219–236, doi:10.1007/s00382-005-0030-7.

Stull, R. B. (1988), *An Introduction to Boundary Layer Meteorology*, Kluwer Acad., Dordrecht, Netherlands.

Tiedtke, M. (1989), A comprehensive mass flux scheme for cumulus parameterization in large-scale models, *Mon. Weather Rev.*, *117*(8), 1779–1800.

Uppala, S. M., et al. (2005), The ERA-40 re-analysis, *Q. J. R. Meteorol. Soc.*, *131*(612), 2961–3012.

von Storch, H. (1995), Misuses of statistical analysis in climate research, in *Analysis of Climate Variability*, edited by H. von Storch and A. Navarra, pp. 11–26, Springer, Berlin.

von Storch, H. (1999), The global and regional climate system, in *Anthropogenic Climate Change*, edited by H. von Storch and G. Flöser, pp. 3–36, Springer, Berlin.

von Storch, H., H. Langenberg, and F. Feser (2000), A spectral nudging technique for dynamical downscaling purposes, *Mon. Weather Rev.*, *128*(10), 3664–3673.

Wan, H., X. L. Wang, and V. R. Swail (2010), Homogenization and trend analysis of Canadian near-surface wind speeds, *J. Clim.*, *23*(5), 1209–1225, doi:10.1175/2009jcli3200.1.

Wang, B. (2006), *The Asian Monsoon*, Springer, Berlin.

Wang, D., C. Menz, T. Simon, C. Simmer, and C. Ohlwein (2013), Regional dynamical downscaling with CCLM over East Asia, *Meteorol. Atmos. Phys.*, *121*(1–2), 39–53, doi:10.1007/s00703-013-0250-z.

Wang, J., and V. R. Kotamarthi (2014), Downscaling with a nested regional climate model in near-surface fields over the contiguous United States, *J. Geophys. Res. Atmos.*, *119*, 8778–8797, doi:10.1002/2014jd021696.

Wentz, F. J., L. Ricciardulli, K. Hilburn, and C. Mears (2007), How much more rain will global warming bring?, *Science*, *317*(5835), 233–235, doi:10.1126/science.1140746.

Winterfeldt, J., and R. Weisse (2009), Assessment of value added for surface marine wind speed obtained from two regional climate models, *Mon. Weather Rev.*, *137*(9), 2955–2965, doi:10.1175/2009MWR2704.1.

Winterfeldt, J., B. Geyer, and R. Weisse (2011), Using QuikSCAT in the added value assessment of dynamically downscaled wind speed, *Int. J. Climatol.*, *31*(7), 1028–1039, doi:10.1002/joc.2105.

Xue, Y., Z. Janjic, J. Dudhia, R. Vasic, and F. De Sales (2014), A review on regional dynamical downscaling in intraseasonal to seasonal simulation/prediction and major factors that affect downscaling ability, *Atmos. Res.*, *147-148*, 68–85, doi:10.1016/j.atmosres.2014.05.001.

Yue, S., P. Pilon, B. Phinney, and G. Cavadias (2002), The influence of autocorrelation on the ability to detect trend in hydrological series, *Hydrol. Processes*, *16*(9), 1807–1829, doi:10.1002/hyp.1095.